Eur. Phys. J. A **16**, 111–125 (2003)
DOI 10.1140/epja/i2002-10071-3

THE EUROPEAN PHYSICAL JOURNAL A

Influence of final-state interaction on incoherent pion photoproduction on the deuteron in the region of the Δ-resonance

E.M. Darwish[a], H. Arenhövel[b], and M. Schwamb

Institut für Kernphysik, Johannes Gutenberg-Universität, D-55099 Mainz, Germany

Received: 12 August 2002 /
Published online: 17 January 2003 –
Communicated by V. Vento

Abstract. The influence of final-state NN and πN rescattering in incoherent pion photoproduction on the deuteron has been investigated. For the elementary photoproduction operator an effective Lagrangian model is used which describes well the elementary reaction. The interactions in the final two-body subsystems are taken in separable form. While NN rescattering shows quite a significant effect, particularly strong for neutral pion production, πN rescattering is almost negligible. Inclusion of such effects leads to an improved and quite satisfactory agreement with experiment.

PACS. 13.60.Le Meson production – 21.45.+v Few-body systems – 25.20.Lj Photoproduction reactions

1 Introduction

The particular interest in pion photoproduction on the deuteron lies in the fact that the simple and well-known deuteron structure allows one to obtain information on the production process on the neutron which otherwise is difficult to obtain in view of the absence of any free neutron targets. The essential idea behind this reasoning is that for quasifree kinematics the dominant production process is given by the elementary reaction on one nucleon, while the other acts merely as a spectator. However, this is possible only if competing two-body processes like final-state interaction (FSI) in the πNN system and possible two-body exchange current contributions are under control.

Early studies of this reaction are done in [1–3]. Approximate treatments of final-state interaction effects within a diagrammatic approach have been reported in [4,5]. In that work, a comparison with experimental data was possible only for π^- production [6], and a satisfactory agreement was found. The authors noted that the FSI effects are quite small for the charged-pion photoproduction reactions in comparison to the neutral channel. More recently Levchuk *et al.* [7] studied quasifree π^0 photoproduction on the neutron via the $d(\gamma,\pi^0)np$ reaction using the elementary photoproduction operator of Blomqvist and Laget [3]. In agreement with the results of [5], they found that the largest rescattering effects arise from the np final-state interaction leading to a strong reduction of the cross-section at pion forward angles, but are much less important in backward direction. The experimental data from [8] for the $d(\gamma,\pi^0)np$ reaction qualitatively support this prediction although a direct comparison was not possible. The threshold region was explored in [9], where a sizeable effect from πN rescattering was noted via intermediate charged-pion production with subsequent charge exchange. Recently, Levchuk *et al.* [10] modified the theoretical predictions of [7] using a more realistic elementary production operator and including also the charged-pion production channels but considering only NN rescattering for which the Bonn r-space potential [11] was used. The elementary production operator was taken from the SAID [12] and MAID [13] multipole analyses. The sizeable effects from NN FSI were confirmed and good agreement with the experimental data was achieved.

The present paper is a natural extension of our work in [14], where this process was studied in the pure impulse approximation (IA), *i.e.*, without inclusion of any FSI or two-body currents. First of all, we were interested in the question whether inclusion of FSI would lead to a good description of the available data, in particular with respect to the recent data on incoherent π^0 production on the deuteron [8]. Although quite a good description was already achieved in [10], we were puzzled by the fact that the results for the IA of this work showed certain significant differences to our IA results [14] for charged-pion production, which is most obvious in the differential cross-sections at forward angles. The origin of this discrep-

[a] *Present address*: Physics Department, Faculty of Science, South Valley University, Sohag, Egypt.
[b] e-mail: arenhoev@kph.uni-mainz.de

ancy was not clear. Furthermore, it was an open question whether the inclusion of rescattering contributions would lead to a different result. Therefore, we have included in the present work as a first step the presumably must important part of the FSI, namely the full hadronic rescattering in all two-body subsystems of the final state, *i.e.*, NN and πN rescattering, whereas the third particle is treated as a spectator. It is still an approximate treatment, the same as in [10], insofar as only the complete scattering in either the NN- or the πN-subsystems are considered, and not a genuine three-body approach. In particular, it will remain a future task to see how critical the violation of unitarity will be.

In the next section we will briefly review the model for the elementary photoproduction amplitude which will serve as an input for the reaction on the deuteron. Section 3 will introduce the general form of the differential cross-section for incoherent pion photoproduction on the deuteron. The separate contributions of the impulse approximation and the two rescatterings to the transition matrix are described in sect. 4. Details of the actual calculation and the results are presented and discussed in sect. 5. Finally, we close in sect. 6 with a summary and an outlook.

2 The elementary pion photoproduction on the nucleon

For the elementary photoproduction operator, we have taken the effective Lagrangian model of Schmidt *et al.* [14] since it is given in an arbitrary frame of reference and allows a well-defined off-shell continuation as required for studying pion production on nuclei. It is in contrast to other approaches, where the elementary amplitude is constructed first on-shell in the photon-nucleon c.m. frame with subsequent boost into an arbitrary reference frame and some prescription for the off-shell continuation. In the latter method, one loses terms which by chance vanish in the c.m. frame [15]. In our approach, the only uncertainty arises from the assignment of the invariant energy for the photon-nucleon subsystem in the resonance propagators as has been discussed in detail in [15]. Here we use the spectator on-shell approach. The model of [14] consists of the standard pseudovector Born terms and the contribution of the $\Delta(1232)$-resonance. For details we refer to [14]. The parameters of the Δ-resonance are fixed by fitting the experimental $M_{1+}^{3/2}$ multipole. With respect to the parameters used in [14], there was only a slight change in the mass of the $\Delta(1232)$-resonance for which we took a value of 1233 MeV. The quality of the model can be judged by a comparison with the MAID analysis [13], the Mainz dispersion analysis [16] and the VPI analysis [12] as shown in fig. 1, and one notes quite a good agreement.

In fig. 2 we compare our results for the differential cross-sections with the MAID analysis [13] and with experimental data. For π^+ and π^0 photoproduction on the proton the data are taken from [17–19] (MAMI), whereas for π^- photoproduction we took the data from [20] (Tokyo). In general, we obtain quite a good agreement with the

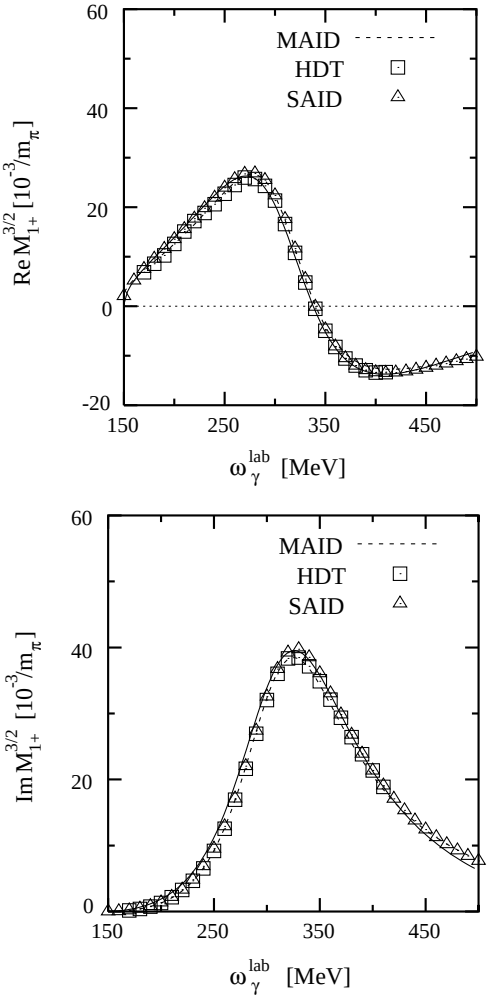

Fig. 1. Real and imaginary parts of the $M_{1+}^{3/2}$ multipole. Notation: solid curves: present model; short-dashed curves: MAID [13]. Data points: from [12] (SAID, solution: September 2000), [16] (HDT).

data, especially in the region of the $\Delta(1232)$-resonance at 330 MeV. Also in comparison with the MAID analysis our elementary production operator does quite well in this energy region. One notes only small discrepancies which very likely come from the fact that no other resonances besides the $\Delta(1232)$ are included in our model.

The total cross-sections for the different pion channels are shown in fig. 3 and compared with experimental data. In general, we obtain a good agreement with the data using the small value $f_{\pi N}^2/4\pi = 0.069$ for the pion-nucleon coupling constant. The agreement with the data from [20] and [21] for π^- photoproduction on the neutron is again satisfactory. In case of the π^+ photoproduction, the agreement is good up to a photon energy of about 400 MeV. For higher energies, the D_{13}-resonance, which is not included in our calculation, gives a non-vanishing contribution [13]. The π^+ data from [20] are slightly underestimated in the resonance region by our calculation but also by the MAID analysis. Except for a tiny overestimation in the maximum, the description of the data for π^0 production on the proton is also very good. Therefore, this model for the el-

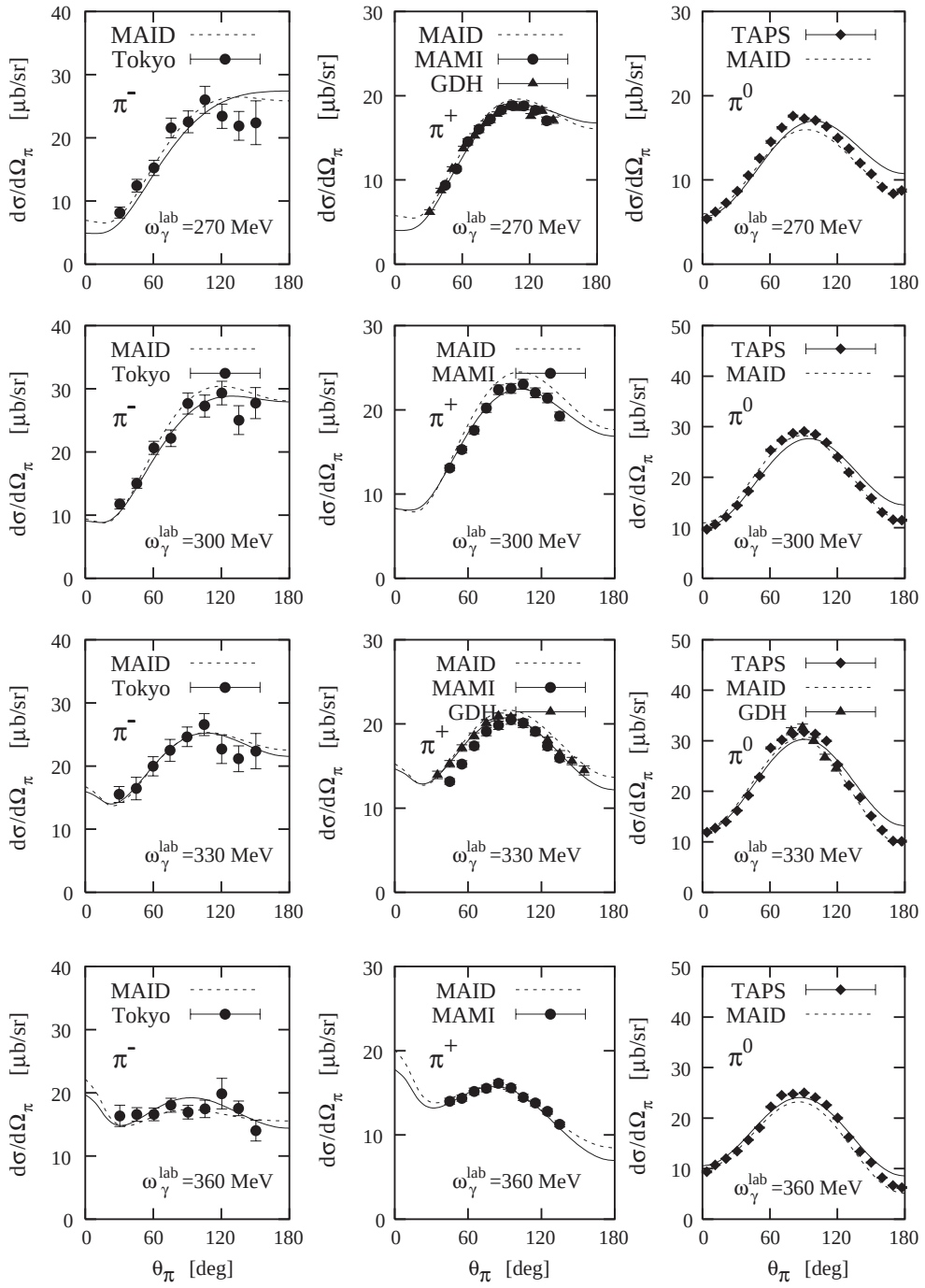

Fig. 2. Differential cross-section for the elementary reaction on the nucleon for the three charge states of the pion at various photon energies. Left panels: π^-, middle panels: π^+, and right panels: π^0. Solid curves: present model; short-dashed curves: MAID [13]. Experimental data from [20] (Tokyo) for π^-, [18] (TAPS), [19] (GDH) for π^0, and [17] (MAMI), [19] (GDH) for π^+.

ementary photoproduction amplitude is quite satisfactory for our purpose, namely to incorporate it into the reaction on the deuteron.

3 Incoherent pion production on the deuteron

We will briefly review the general formalism for incoherent pion production on the deuteron. The general expression for the unpolarized differential cross-section of pion photoproduction reaction on the deuteron is given, using the conventions of Bjorken and Drell [23], by

$$\begin{aligned} \mathrm{d}\sigma = {} & (2\pi)^{-5}\delta^4(k+d-p_1-p_2-q) \\ & \times \frac{1}{|\vec{v}_\gamma - \vec{v}_d|}\frac{1}{2}\frac{\mathrm{d}^3q}{2\omega_{\vec{q}}}\frac{\mathrm{d}^3p_1}{E_1}\frac{\mathrm{d}^3p_2}{E_2}\frac{M_N^2}{4\omega_\gamma E_d}\frac{1}{6} \\ & \times \sum_{s,m,t,m_\gamma,m_d} |\mathcal{M}^{(t\mu)}_{sm\,m_\gamma m_d}|^2, \end{aligned} \tag{1}$$

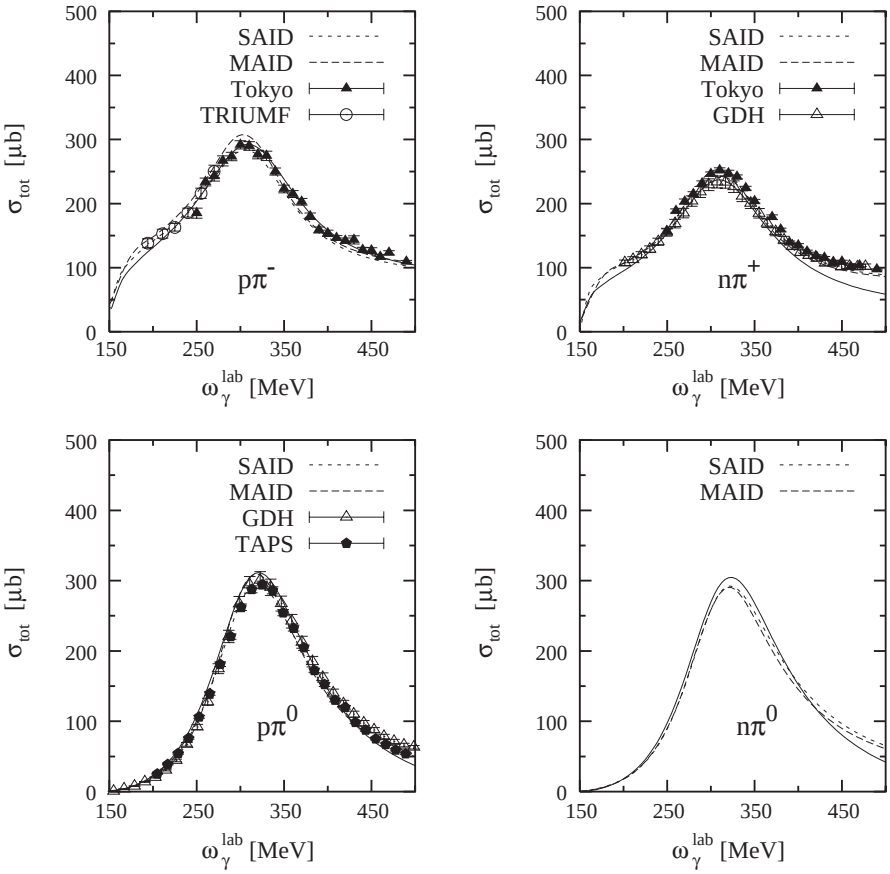

Fig. 3. Total cross-sections for pion photoproduction on the nucleon as a function of photon energy for all four physical channels. Notation of the curves: solid: present model; short-dashed: SAID [12]; dashed: MAID [13]. Experimental data from [20] (Tokyo), [21] (TRIUMF), [19] (GDH), [22] (TAPS).

where initial photon and deuteron four-momenta are denoted by $k = (\omega_\gamma, \vec{k})$ and $d = (E_d, \vec{d})$, respectively, and the four-momenta of final meson and two nucleons by $q = (\omega_q, \vec{q})$ with $\omega_q = \sqrt{m_\pi^2 + \vec{q}^2}$, m_π as pion mass, and $p_j = (E_j, \vec{p}_j)$ $(j = 1, 2)$ with $E_j = \sqrt{M_N^2 + \vec{p}_j^{\,2}}$, respectively, and M_N as nucleon mass. Furthermore, m_γ denotes the photon polarization, m_d the spin projection of the deuteron, s and m total spin and projection of the two outgoing nucleons, respectively, t their total isospin, μ the isospin projection of the pion, and $\vec{v}_\gamma$ and $\vec{v}_d$ the velocities of photon and deuteron, respectively. The states of all particles are covariantly normalized. The reaction amplitude is denoted by $\mathcal{M}^{(t\mu)}_{s\,m m_\gamma m_d}$. As in [14], we have chosen as independent variables the pion momentum q, its angles θ_π and ϕ_π, the polar angle $\theta_{p_{NN}}$ and the azimuthal angle $\phi_{p_{NN}}$ of the relative momentum $\vec{p}_{NN}$ of the two outgoing nucleons as independent variables.

The total and relative momenta of the final NN-system are defined, respectively, by

$$\vec{P}_{NN} = \vec{p}_1 + \vec{p}_2 = \vec{k} - \vec{q}$$

and

$$\vec{p}_{NN} = \frac{1}{2}(\vec{p}_1 - \vec{p}_2). \tag{2}$$

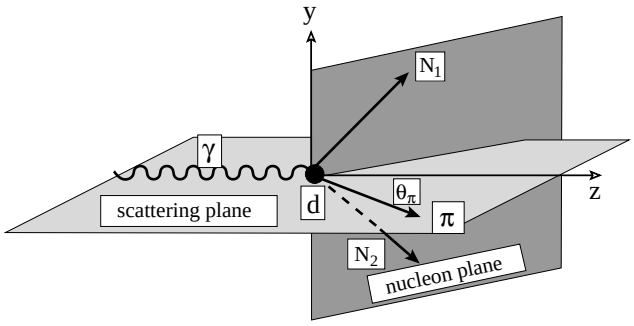

Fig. 4. Kinematics in the laboratory system for $\gamma d \to \pi NN$.

The absolute value of the relative momentum $\vec{p}_{NN}$ is given by

$$p_{NN} = \frac{1}{2}\sqrt{\frac{E_{NN}^2(W_{NN}^2 - 4M_N^2)}{E_{NN}^2 - P_{NN}^2\cos^2\theta_{P p_{NN}}}}\,, \tag{3}$$

where E_{NN} and W_{NN} denote total energy and invariant mass of the NN-subsystem

$$\begin{aligned} E_{NN} &= E_1 + E_2 = \omega_\gamma + E_d - \omega_q, \\ W_{NN}^2 &= E_{NN}^2 - P_{NN}^2, \end{aligned} \tag{4}$$

$$\rho_s = \frac{1}{(2\pi)^5} \frac{p_{NN}^2 M_N^2}{|E_2(p_{NN} + \frac{1}{2}P_{NN}\cos\theta_{P_{p_{NN}}}) + E_1(p_{NN} - \frac{1}{2}P_{NN}\cos\theta_{P_{p_{NN}}})|} \frac{q^2}{16\,\omega_\gamma M_d\,\omega_q}\,. \tag{7}$$

and $\theta_{P_{p_{NN}}}$ is the angle between $\vec{P}_{NN}$ and $\vec{p}_{NN}$.

For the evaluation we have chosen the laboratory frame where $d^\mu = (M_d, \vec{0})$ with M_d as deuteron mass. As coordinate system a right-handed one is taken with z-axis along the momentum $\vec{k}$ of the incoming photon and y-axis along $\vec{k}\times\vec{q}$. Thus, the outgoing pion defines the scattering plane. Another plane is defined by the momenta of the outgoing nucleons which we will call the nucleon plane (see fig. 4).

In the later discussion of the main features of the processes we will consider the semi-inclusive differential cross-section $\mathrm{d}^2\sigma/\mathrm{d}\Omega_\pi$, where only the final pion is detected. It is obtained from the fully exclusive cross-section

$$\frac{\mathrm{d}^5\sigma}{\mathrm{d}\Omega_{p_{NN}}\,\mathrm{d}\Omega_\pi\,\mathrm{d}q} = \frac{\rho_s}{6} \sum_{s,m,t,m_\gamma,m_d} |\mathcal{M}^{(t\mu)}_{s\,m\,m_\gamma m_d}|^2 \tag{5}$$

by integration over q and $\Omega_{p_{NN}}$

$$\frac{\mathrm{d}^2\sigma}{\mathrm{d}\Omega_\pi} = \int_0^{q_{\max}} \mathrm{d}q \int \mathrm{d}\Omega_{p_{NN}} \frac{\mathrm{d}^5\sigma}{\mathrm{d}\Omega_{p_{NN}}\,\mathrm{d}\Omega_\pi\,\mathrm{d}q}\,, \tag{6}$$

where the maximal pion momentum $q_{\max}$ is determined by the kinematics. The phase space factor ρ_s in (5) is expressed in terms of relative and total momenta of the two final nucleons

see eq. (7) *above.*

4 The transition matrix

The general form of the photoproduction transition matrix is given by

$$\mathcal{M}^{(t\mu)}_{s\,m\,m_\gamma m_d}\big(\vec{k},\vec{q},\vec{p_1},\vec{p_2}\big) = {}^{(-)}\big\langle \vec{q}\,\mu, \vec{p_1}\vec{p_2}\; s\,m\,t-\mu\big|\epsilon_\mu(m_\gamma)J^\mu(0)\big|\vec{d}\,m_d\,00\big\rangle, \tag{8}$$

where $J^\mu(0)$ denotes the current operator and $\epsilon_\mu(m_\gamma)$ the photon polarization vector. The electromagnetic interaction consists of the elementary production process on one of the nucleons $T^{(j)}_{\pi\gamma}$ $(j=1,2)$ and in principle a possible irreducible two-body production operator $T^{(NN)}_{\pi\gamma}$. The final πNN state is then subject to the various hadronic two-body interactions as described by an half-off-shell three-body scattering amplitude $T^{\pi NN}$. In the following, we will neglect the electromagnetic two-body production $T^{(NN)}_{\pi\gamma}$, and the outgoing πNN scattering state is approximated in this work by

$$|\vec{q}\,\mu, \vec{p_1}\vec{p_2}\; s\,m\,t-\mu\rangle^{(-)} = |\vec{q}\,\mu, \vec{p_1}\vec{p_2}\; s\,m\,t-\mu\rangle + G_0^{\pi NN(-)}\big(T^{\pi N}(1) + T^{\pi N}(2) + T^{NN}\big) \times|\vec{q}\,\mu, \vec{p_1}\vec{p_2}\; s\,m\,t-\mu\rangle\,, \tag{9}$$

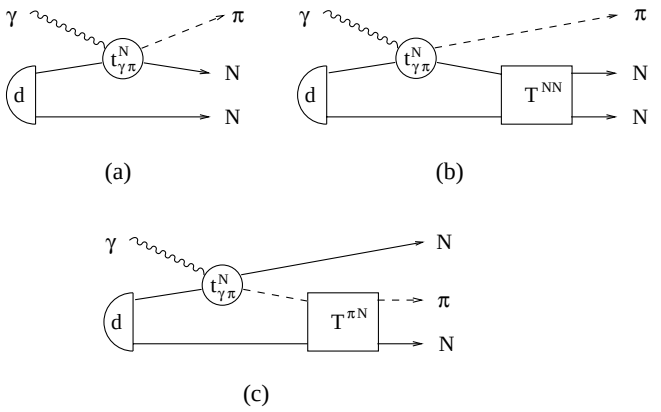

Fig. 5. Diagramatic representation of $\gamma d \to \pi NN$ including rescattering in the two-body subsystems of the final state: (a) impulse approximation (IA), (b) NN rescattering, and (c) πN rescattering.

where $|\vec{q}\,\mu, \vec{p_1}\vec{p_2}\; s\,m\,t-\mu\rangle$ denotes the free πNN plane wave, $G_0^{\pi NN(-)}$ the free πNN propagator, $T^{\pi N}(j)$ the reaction operator for πN scattering on nucleon "j", and T^{NN} the corresponding one for NN scattering. This means, we include besides the pure impulse approximation (IA), which is defined by the e.m. pion production on one of the nucleons alone, only the complete rescattering by the final-state interaction within each of the two-body subsystems. Therefore, the total transition matrix element reads in this approximation

$$\mathcal{M}^{(t\mu)}_{s\,m\,m_\gamma m_d} = \mathcal{M}^{(t\mu)\,\mathrm{IA}}_{s\,m\,m_\gamma m_d} + \mathcal{M}^{(t\mu)\,NN}_{s\,m\,m_\gamma m_d} + \mathcal{M}^{(t\mu)\,\pi N}_{s\,m\,m_\gamma m_d}, \tag{10}$$

in an obvious notation. A graphical representation of the transition matrix is shown in fig. 5. We will now consider the different contributions in detail.

4.1 The impulse approximation

Here we briefly review the relevant formulae from [14]. In the IA the final-state interaction is neglected and the pion and the NN final states are described by pure plane waves (see fig. 5(a)). For the spin ($|sm\rangle$) and isospin ($|t-\mu\rangle$) part of the two-nucleon wave functions we use a coupled spin-isospin basis $|sm,\, t{-}\mu\rangle$. The antisymmetric final NN plane-wave function thus has the form

$$|\vec{p}_1,\vec{p}_2,sm,t-\mu\rangle = \frac{1}{\sqrt{2}}\big(|\vec{p}_1\rangle^{(1)}|\vec{p}_2\rangle^{(2)} - (-)^{s+t}|\vec{p}_2\rangle^{(1)}|\vec{p}_1\rangle^{(2)}\big)|sm\,,t-\mu\rangle, \tag{11}$$

where the superscript indicates to which particle the ket refers. In the case of charged pions, only the $t=1$ channel

contributes, whereas for π^0 production both $t = 0$ and $t = 1$ channels have to be taken into account. Then the IA matrix element is given by

$$\begin{aligned}
&\mathcal{M}^{(t\mu)\ \mathrm{IA}}_{s\,m\,m_\gamma m_d}(\vec{k},\vec{q},\vec{p_1},\vec{p_2}) = \\
&\langle \vec{p}_1,\vec{p}_2,sm,t-\mu|t^{NN}_{\gamma\pi}(\vec{k},\vec{q})|\vec{d}m_d,00\rangle = \\
&\frac{1}{2}\int\frac{\mathrm{d}^3p_1'}{(2\pi)^3}\int\frac{\mathrm{d}^3p_2'}{(2\pi)^3}\frac{M_N^2}{E_1'E_2'} \\
&\times\sum_{m'}\langle\,\vec{p}_1\vec{p}_2,sm,t-\mu|\,t^{NN}_{\gamma\pi}(\vec{k},\vec{q})\,|\,\vec{p}_1'\vec{p}_2',1m',00\rangle \\
&\times\langle\,\vec{p}_1'\vec{p}_2',1m',00\mid\vec{d}m_d,\,00\rangle \qquad (12)
\end{aligned}$$

with

$$t^{NN}_{\gamma\pi}(\vec{k},\vec{q}) = t^{N(1)}_{\gamma\pi}(\vec{k},\vec{q}) + t^{N(2)}_{\gamma\pi}(\vec{k},\vec{q})\,, \qquad (13)$$

where $t^{N(j)}_{\gamma\pi}$ denotes the elementary production amplitude on nucleon "j". As mentioned above, we use covariant normalization for the nucleon, deuteron and meson states, *i.e.*,

$$\begin{aligned}
\langle\vec{p}\,'\mid\vec{p}\,\rangle &= (2\pi)^3\frac{E_p}{M_N}\,\delta^3(\vec{p}\,'-\vec{p}), \\
\langle\vec{d}\,'\mid\vec{d}\,\rangle &= (2\pi)^3 2E_d\,\delta^3(\vec{d}\,'-\vec{d}\,)\,, \\
\langle\vec{q}\,'\mid\vec{q}\,\rangle &= (2\pi)^3\,2\,\omega_q\,\delta(\vec{q}\,'-\vec{q}\,)\,. \qquad (14)
\end{aligned}$$

The deuteron wave function has the form

$$\begin{aligned}
\langle\,\vec{p}_1\vec{p}_2,1m,\,00\mid\vec{d}m_d,00\rangle &= (2\pi)^3\delta^3\big(\vec{d}-\vec{p}_1-\vec{p}_2\big) \\
&\times\frac{\sqrt{2E_1E_2}}{M_N}\widetilde{\Psi}_{m,m_d}(\vec{p}_{NN}) \qquad (15)
\end{aligned}$$

with

$$\begin{aligned}
\widetilde{\Psi}_{m,m_d}(\vec{p}) &= (2\pi)^{\frac{3}{2}}\sqrt{2E_d}\sum_{L=0,2}\sum_{m_L} i^L\,C^{L11}_{m_L m m_d} \\
&\times u_L(p)Y_{Lm_L}(\hat{p})\,, \qquad (16)
\end{aligned}$$

denoting with $C^{j_1j_2j}_{m_1m_2m}$ a Clebsch-Gordan coefficient. Using (13), one finds in the laboratory system for the IA matrix element the following expression:

$$\begin{aligned}
&\mathcal{M}^{(t\mu)\ \mathrm{IA}}_{s\,m\,m_\gamma m_d}(\vec{k},\vec{q},\vec{p_1},\vec{p_2}) = \\
&\quad\sqrt{2}\sum_{m'}\langle sm,\,t-\mu|\Big(\langle\vec{p}_1|t^{N(1)}_{\gamma\pi}(\vec{k},\vec{q})|-\vec{p}_2\rangle \\
&\quad\times\tilde{\Psi}_{m',m_d}(\vec{p}_2)-(-)^{s+t}(\vec{p_1}\longleftrightarrow\vec{p_2})\Big)|1m',\,00\rangle. \qquad (17)
\end{aligned}$$

Note that in (17) the elementary production operator acts on nucleon "1" only. This matrix element possesses the obvious symmetry under the interchange of the nucleon momenta

$$\begin{aligned}
&\mathcal{M}^{(t\mu)\,\mathrm{IA}}_{s\,m\,m_\gamma m_d}(\vec{k},\vec{q},\vec{p_2},\vec{p_1}) = \\
&\quad(-)^{s+t+1}\mathcal{M}^{(t\mu)\,\mathrm{IA}}_{s\,m\,m_\gamma m_d}(\vec{k},\vec{q},\vec{p_1},\vec{p_2}). \qquad (18)
\end{aligned}$$

4.2 NN rescattering

As next we will evaluate the NN rescattering contribution whose Feynman diagram is shown in fig. 5(b). The transition matrix element has the form

$$\begin{aligned}
\mathcal{M}^{(t\mu)\ NN}_{s\,m\,m_\gamma m_d} &= \frac{1}{2}\int\frac{\mathrm{d}^3p_1'}{(2\pi)^3}\int\frac{\mathrm{d}^3p_2'}{(2\pi)^3}\frac{M_N^2}{E_1'E_2'}\sum_{m'}\mathcal{R}^{NN,\,t\mu}_{s\,mm'} \\
&\times(W_{NN},\vec{p}_1,\vec{p}_2,\vec{p}_1',\vec{p}_2')\,\mathcal{G}_0^{\pi NN(+)}(E_{\gamma d},\vec{q},\vec{p}_1',\vec{p}_2') \\
&\times\mathcal{M}^{(t\mu)\ \mathrm{IA}}_{sm'm_\gamma m_d}(\vec{k},\vec{q},\vec{p}_1',\vec{p}_2'). \qquad (19)
\end{aligned}$$

Here $\mathcal{R}^{NN,\,t\mu}(W_{NN})$ contains the half-off-shell NN scattering matrix at the invariant energy of the NN-subsystem W_{NN}, and $\mathcal{G}_0^{\pi NN(+)}(E_{\gamma d},\vec{q},\vec{p}_1',\vec{p}_2')$ denotes the free πNN propagator. The latter is given by

$$\begin{aligned}
&\mathcal{G}_0^{\pi NN(+)}(E_{\gamma d},\vec{q},\vec{p}_1',\vec{p}_2') = \\
&\quad\big(E_{\gamma d}-\omega_\pi(\vec{q})-E_1(\vec{p}_1')-E_2(\vec{p}_2')+i\epsilon\big)^{-1}, \qquad (20)
\end{aligned}$$

where $E_{\gamma d} = \omega_\gamma + M_d$. Now we introduce relative and total momenta $\vec{p}^{\,(\prime)}_{NN}$ and $\vec{P}^{\,(\prime)}$, respectively, of the interacting nucleons in initial and final states

$$\vec{p}^{\,(\prime)}_{NN} = \frac{1}{2}\Big(\vec{p}_1^{\,(\prime)}-\vec{p}_2^{\,(\prime)}\Big), \qquad \vec{P}^{(\prime)} = \vec{p}_1^{\,(\prime)}+\vec{p}_2^{\,(\prime)}. \qquad (21)$$

Using non-relativistic kinematics for the nucleons, one finds for the propagator

$$\mathcal{G}_0^{\pi NN(+)}(E_{\gamma d},\vec{q},\vec{p}_1',\vec{p}_2') = \frac{M_N}{\widetilde{p}^{\,2}-p_{NN}'^2+i\epsilon}\,, \qquad (22)$$

where $\widetilde{p}$ is given by

$$\widetilde{p}^{\,2} = M_N\bigg(E_{\gamma d}-\omega_\pi(\vec{q})-2M_N-\frac{(\vec{k}-\vec{q}\,)^2}{4M_N}\bigg). \qquad (23)$$

As next we separate the c.m. motion of the two-nucleon subsystem and obtain for the NN rescattering amplitude $\mathcal{R}^{NN}$

$$\begin{aligned}
&\mathcal{R}^{NN,\,t\mu}_{smm'}(W_{NN},\vec{p}_1,\vec{p}_2,\vec{p}_1',\vec{p}_2') = \\
&\quad 2(2\pi)^6\delta^3(\vec{P}\,'-\vec{P})\frac{\sqrt{E_1E_2E_1'E_2'}}{M_N^2} \\
&\quad\times\widetilde{\mathcal{R}}^{NN,\,t\mu}_{smm'}(W_{NN},\vec{p}_{NN},\vec{p}\,'_{NN}). \qquad (24)
\end{aligned}$$

Here we have introduced the conventional NN scattering matrix $\widetilde{\mathcal{R}}^{NN,\,t\mu}_{s\,mm'}$ with respect to non-covariantly normalized states, which is expanded in terms of the partial wave contributions $\mathcal{T}^{NN,\,t\mu}_{Js\ell\ell'}$

$$\begin{aligned}
&\widetilde{\mathcal{R}}^{NN,\,t\mu}_{s\,mm'}(W_{NN},\vec{p}_{NN},\vec{p}\,'_{NN}) = \\
&\sum_{J\ell\ell'}\mathcal{F}^{NN,\,Js}_{\ell\ell'\,mm'}(\hat{p}_{NN},\hat{p}\,'_{NN})\mathcal{T}^{NN,\,t\mu}_{Js\ell\ell'}(W_{NN},p_{NN},p'_{NN}), \qquad (25)
\end{aligned}$$

where orbital and total angular momenta of the two-nucleon system are denoted by ℓ and J, respectively. The

purely angular function $\mathcal{F}^{NN,\,Js}_{\ell\ell' mm'}(\hat{p}_{NN},\hat{p}'_{NN})$ is defined by

$$\mathcal{F}^{NN,\,Js}_{\ell\ell' mm'}(\hat{p}_{NN},\hat{p}'_{NN}) = \sum_{M m_\ell m_{\ell'}} C^{\ell s J}_{m_\ell m M}\, C^{\ell' s J}_{m_{\ell'} m' M} \times Y^{\star}_{\ell m_\ell}(\hat{p}_{NN}) Y_{\ell' m_{\ell'}}(\hat{p}'_{NN}). \quad (26)$$

Collecting the various pieces and substituting (24) and (22) into (19), one obtains the following expression for the NN rescattering contribution:

$$\mathcal{M}^{(t\mu)\,NN}_{s\,m\,m_\gamma m_d}(\vec{k},\vec{q},\vec{p}_1,\vec{p}_2) = \sum_{m'} \int \mathrm{d}^3\vec{p}'_{NN} \sqrt{\frac{E_1 E_2}{E'_1 E'_2}}\, \widetilde{\mathcal{R}}^{NN,t\mu}_{smm'}(W_{NN},\vec{p}_{NN},\vec{p}'_{NN}) \times \frac{M_N}{\widetilde{p}^{\,2} - p'^{\,2}_{NN} + i\epsilon}\, \mathcal{M}^{(t\mu)\,\mathrm{IA}}_{s\,m',m_\gamma m_d}(\vec{k},\vec{q},\vec{p}'_1,\vec{p}'_2), \quad (27)$$

where $\vec{p}'_{1/2} = \pm\vec{p}'_{NN} + (\vec{k}-\vec{q})/2$ and $E'_{1/2}$ the corresponding on-shell energies.

4.3 πN rescattering

The last contribution concerns the πN rescattering in the final state whose diagram is shown in fig. 5(c). The corresponding transition matrix element has formally a similar structure as the one for NN rescattering and is given by

$$M^{(t\mu)\pi N}_{s\,m,m_\gamma m_d}(\vec{k},\vec{q},\vec{p}_1,\vec{p}_2) = \frac{1}{2}\sum_{\alpha'} \int \frac{\mathrm{d}^3\vec{q}'}{(2\pi)^3} \frac{\mathrm{d}^3\vec{p}'_1}{(2\pi)^3} \frac{\mathrm{d}^3\vec{p}'_2}{(2\pi)^3} \frac{M_N^2}{2\omega_{q'} E'_1 E'_2} \times \Big[\mathcal{R}^{\pi N}_{\alpha\alpha'}(\vec{q},\vec{p}_1,\vec{p}_2,\vec{q}',\vec{p}'_1,\vec{p}'_2) - (-)^{s+t}\mathcal{R}^{\pi N}_{\alpha\alpha'}(\vec{q},\vec{p}_2,\vec{p}_1,\vec{q}',\vec{p}'_1,\vec{p}'_2)\Big] \times \mathcal{G}^{\pi NN(+)}_0(E_{\gamma d},\vec{q}',\vec{p}'_1,\vec{p}'_2)\, \mathcal{M}^{(t'\mu')\,\mathrm{IA}}_{s'm'm_\gamma m_d} \times (\vec{k},\vec{q}',\vec{p}'_1,\vec{p}'_2), \quad (28)$$

where we have introduced as a shorthand for the quantum numbers $\alpha = (s\,m t\mu)$ and have made use of the symmetry (18). Furthermore, $\mathcal{R}^{\pi N}_{\alpha\alpha'}(\vec{q},\vec{p}_1,\vec{p}_2,\vec{q}',\vec{p}'_1,\vec{p}'_2)$ contains the half-off-shell πN scattering matrix. Separating the non-participating spectator nucleon and the c.m. motion of the interacting πN-subsystem, switching to an uncoupled spin-isospin basis, and coupling the isospins of the interacting pion and nucleon to a total isospin $\tilde{t}$, one obtains

$$\mathcal{R}^{\pi N}_{\alpha\alpha'}(\vec{q},\vec{p}_1,\vec{p}_2,\vec{q}',\vec{p}'_1,\vec{p}'_2) = (2\pi)^9\, 2\sqrt{\omega_q\omega_{q'}}\, \frac{E_1}{M_N} \sqrt{\frac{E_2 E'_2}{M_N^2}}\, \delta(\vec{p}_1-\vec{p}'_1) \times \delta(\vec{q}+\vec{p}_2-\vec{q}'-\vec{p}'_2) \times \sum_{m_2 m'_2}\sum_{\mu_2\mu'_2}\sum_{\tilde{t}\tilde{\mu}} \mathcal{C}^{\tilde{t}\tilde{\mu}}_{\alpha\alpha'}(m_2,m'_2,\mu_2,\mu'_2) \times \widetilde{\mathcal{R}}^{\pi N,\,\tilde{t}\tilde{\mu}}_{m_2 m'_2}(W_{\pi N}(\vec{p}_2),\vec{p}_{\pi N},\vec{p}'_{\pi N}), \quad (29)$$

where

$$\mathcal{C}^{\tilde{t}\tilde{\mu}}_{\alpha\alpha'}(m_2,m'_2,\mu_2,\mu'_2) = C^{1\frac{1}{2}\tilde{t}}_{\mu\mu_2\tilde{\mu}}\, C^{1\frac{1}{2}\tilde{t}}_{\mu'\mu'_2\tilde{\mu}} \times \sum_{m_1} C^{\frac{1}{2}\frac{1}{2}s}_{m_1 m_2 m}\, C^{\frac{1}{2}\frac{1}{2}s}_{m_1 m'_2 m'} \times \sum_{\mu_1} C^{\frac{1}{2}\frac{1}{2}t}_{\mu_1\mu_2-\mu}\, C^{\frac{1}{2}\frac{1}{2}t'}_{\mu_1\mu'_2-\mu'} \quad (30)$$

contains the recoupling coefficients, and $\widetilde{\mathcal{R}}^{\pi N,\,\tilde{t}\tilde{\mu}}_{m_2 m'_2}$ denotes the half-off-shell πN scattering matrix at the invariant mass $W_{\pi N}(\vec{p}_2) = \sqrt{(E_2+\omega_q)^2 - (\vec{q}+\vec{p}_2)^2}$ of the πN-subsystem. Furthermore, m_2 (m'_2) and μ_2 (μ'_2) denote the spin and isospin projections of the final (initial) nucleon in the πN-subsystem, respectively. The relative momentum of the final (initial) pion-nucleon subsystem is given, respectively, by

$$\vec{p}_{\pi N} = \frac{M_N\vec{q} - m_\pi\vec{p}_2}{M_N+m_\pi}, \qquad \vec{p}'_{\pi N} = \frac{M_N\vec{q}' - m_\pi\vec{p}'_2}{M_N+m_\pi} = \frac{M_N}{M_N+m_\pi}(\vec{q}+\vec{p}_2) - \vec{p}'_2\,. \quad (31)$$

The πN scattering matrix is now expanded in terms of partial-wave amplitudes

$$\widetilde{\mathcal{R}}^{\pi N,\,\tilde{t}\tilde{\mu}}_{m_2 m'_2}(W_{\pi N}(\vec{p}_2),\vec{p}_{\pi N},\vec{p}'_{\pi N}) = \sum_{J\ell} \mathcal{F}^{\pi N}_{J\ell m_2 m'_2}(\hat{p}_{\pi N},\hat{p}'_{\pi N})\, \mathcal{T}^{\pi N,\,\tilde{t}\tilde{\mu}}_{J\ell} \times (W_{\pi N}(\vec{p}_2),p_{\pi N},p'_{\pi N})\,, \quad (32)$$

where we have defined

$$\mathcal{F}^{\pi N}_{J\ell m_2 m'_2}(\hat{p}_{\pi N},\hat{p}'_{\pi N}) = \sum_{m_\ell m'_\ell M} C^{\frac{1}{2}\ell J}_{m_2 m_\ell M}\, C^{\frac{1}{2}\ell J}_{m'_2 m'_\ell M}\, Y^{\star}_{\ell m_\ell}(\hat{p}_{\pi N}) Y_{\ell m'_\ell}(\hat{p}'_{\pi N}). \quad (33)$$

Inserting (29) with (32) into (28), one obtains the final form for the πN rescattering contribution

$$M^{(t\mu)\pi N}_{s\,m\,m_\gamma m_d}(\vec{k},\vec{q},\vec{p}_1,\vec{p}_2) = \frac{1}{2}\sum_{\alpha'} \int \mathrm{d}^3\vec{p}'_2 \sqrt{\frac{\omega_q\, E_2}{\omega_{q'}\, E'_2}} \sum_{m_2 m'_2}\sum_{\mu_2\mu'_2}\sum_{\tilde{t}\tilde{\mu}} \mathcal{C}^{\tilde{t}\tilde{\mu}}_{\alpha\alpha'}(m_2,m'_2,\mu_2,\mu'_2) \times \Bigg[\sum_{J\ell} \mathcal{F}^{\pi N}_{J\ell m_2 m'_2}(\hat{p}_{\pi N},\hat{p}'_{\pi N})\, \mathcal{T}^{\pi N,\,\tilde{t}\tilde{\mu}}_{J\ell} \times (W_{\pi N}(\vec{p}_2),p_{\pi N},p'_{\pi N})\, \mathcal{G}^{\pi NN(+)}_0(E_{\gamma d},\vec{q}',\vec{p}_1,\vec{p}'_2) \times \mathcal{M}^{(t'\mu')\,\mathrm{IA}}_{s'm',m_\gamma m_d}(\vec{k},\vec{q}',\vec{p}_1,\vec{p}'_2) - (-)^{s+t}(\vec{p}_1\leftrightarrow\vec{p}_2)\Bigg], \quad (34)$$

where $\vec{p}'_{\pi N}$ and $\vec{p}_{\pi N}$ are given in (31) and $\vec{q}' = \vec{q}+\vec{p}_2-\vec{p}'_2$.

5 Results and discussion

The three contributions to the pion production amplitude, *i.e.*, the IA in (17) and the two rescattering contributions

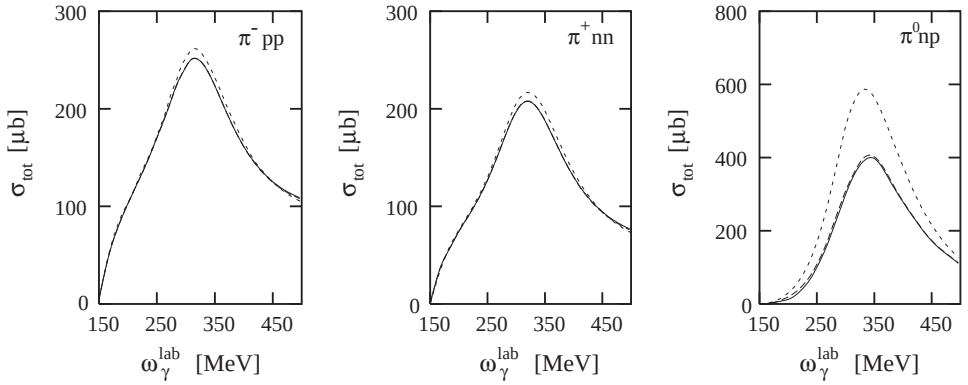

Fig. 6. Total cross-sections for $\gamma d \to \pi NN$. Notation of curves: short-dashed: impulse approximation (IA); dashed: IA plus NN rescattering; solid: IA plus NN and πN rescattering. The left, middle and right panels represent the results for $\gamma d \to \pi^- pp$, $\pi^+ nn$ and $\pi^0 np$, respectively.

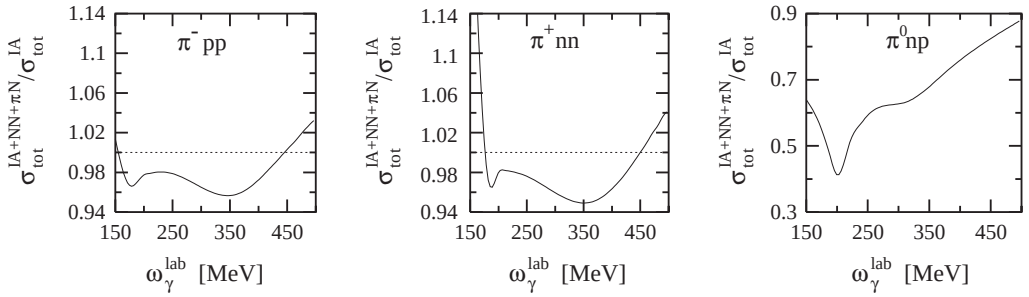

Fig. 7. The ratio of the total cross-section with complete rescattering $\sigma_{\rm tot}^{{\rm IA}+NN+\pi N}$ to the one in the IA $\sigma_{\rm tot}^{\rm IA}$ as a function of the lab photon energy. The left, middle and right panels represent the ratios for π^-, π^+ and π^0 production, respectively.

in (27) and (34) are evaluated by taking a realistic NN potential model for the deuteron wave function and the NN scattering amplitudes, in this work the Paris potential. Specifically, we have taken the deuteron wave function from [24] and the interaction in the separable representation of [25,26]. Explicitly, we have included all partial waves with total angular momentum $J \leq 3$. Also in the case of πN rescattering we have used the separable energy-dependent πN potential of [27] and have considered all S-, P- and D-waves. The remaining three-dimensional integrals in (27) over $\vec{p}\,'_{NN}$ and in (34) over $\vec{p}\,'_2$ are evaluated numerically. We would like to remark, that we have obtained essentially the same results if we take the Bonn r-space potential [11] instead of the Paris one.

The discussion of our results is divided into two parts. First, we will discuss the influence of FSI on the total cross-section by comparing the pure IA with the inclusion of two-body rescattering in the final state. Furthermore, we will confront our results with experimental data and other theoretical calculations. In the second part, we will then consider the semi-exclusive differential cross-section $\mathrm{d}^2\sigma/\mathrm{d}\Omega_\pi$, where only the pion is detected in the final state.

5.1 Total cross-section

Our results for the total cross-sections in IA alone and with FSI effects included are presented in fig. 6. In order to show in greater detail the relative influence of rescattering effects on the total cross-sections, we show in fig. 7 the effect of complete rescattering relative to the IA by the ratio $\sigma_{\rm tot}^{{\rm IA}+NN+\pi N}/\sigma_{\rm tot}^{\rm IA}$ and in fig. 8 the effect of πN rescattering alone relative to the complete effect by the ratio $\sigma_{\rm tot}^{{\rm IA}+NN+\pi N}/\sigma_{\rm tot}^{{\rm IA}+NN}$, where $\sigma_{\rm tot}^{\rm IA}$ denotes the total cross-section in the impulse approximation, $\sigma_{\rm tot}^{{\rm IA}+NN}$ the one including only NN rescattering, and $\sigma_{\rm tot}^{{\rm IA}+NN+\pi N}$ the one including in addition πN rescattering contributions. One readily notes the importance of rescattering effects, in particular for the π^0 channel. FSI leads in all cases, to a reduction of the total cross-section, except close to the production threshold, where for charged pions one notes a sizeable increase and above about 450 MeV. The sizeable effect of πN rescattering in the threshold region confirms the previous results in [3] for the coherent reaction and in [9,28] for the incoherent one. Furthermore, it has been pointed out already in [9], that also for charged-pion channels rescattering effects are important in the threshold region.

In the energy range of the $\Delta(1232)$-resonance, one finds the strongest reduction by rescattering effects which arise predominantly from NN rescattering, whereas the influence of πN rescattering appears almost negligible, about an order of magnitude smaller, as is evident from fig. 8. Only for neutral pion production πN rescattering becomes noticable below the Δ region and amounts to about 40% of the total effect near 175 MeV. The reason

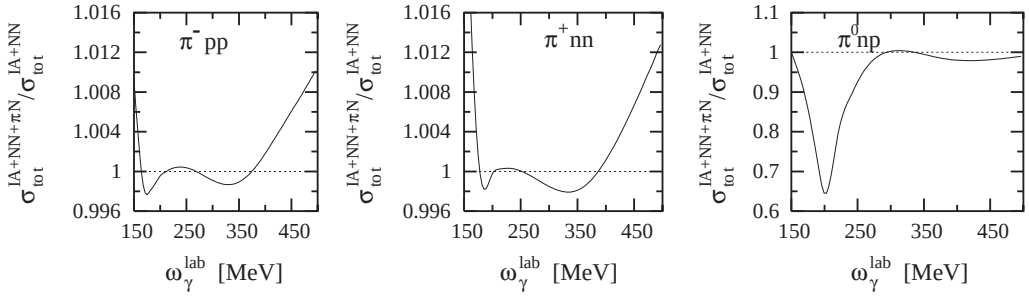

Fig. 8. The ratio of the total cross-section with complete rescattering $\sigma_{\rm tot}^{{\rm IA}+NN+\pi N}$ to the one, where only NN rescattering is included, $\sigma_{\rm tot}^{{\rm IA}+NN}$ as function of the lab photon energy. The left, middle and right panels represent the ratios for π^-, π^+ and π^0 production, respectively.

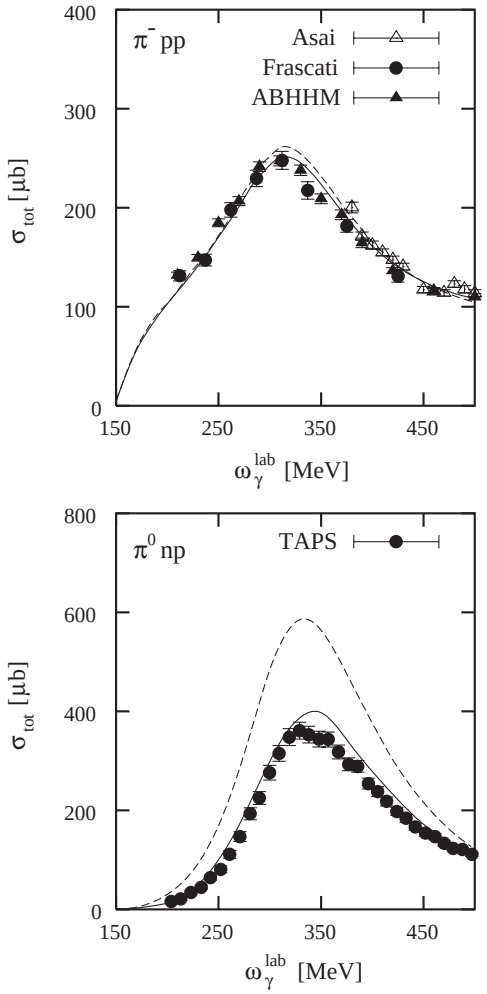

Fig. 9. Total cross-sections for π^- (upper panel) and π^0 (lower panel) photoproduction on the deuteron. Solid curves: our results with NN and πN rescattering; dashed curves: impulse approximation. Experimental data from [6] (ABHHM), [29] (Frascati) and [30] (Asai) for π^-, and from [8] (TAPS) for π^0 production.

for this relatively small effect from πN rescattering lies in the much smaller πN interaction in comparison to the NN interaction. This is manifest by the fact that the S-wave scattering length of πN scattering is about two orders of magnitude smaller than the one of NN scattering.

While for charged-pion photoproduction FSI effects are relatively small, not more than about 5%, they are quite strong in the case of neutral pion photoproduction, reaching a maximum of about 60% at 175 MeV and still about 35% in the Δ region. The large NN FSI effect in neutral pion production has two related sources. The first arises from the fact that for the π^0 channel the IA contains a contribution from the coherent process because the final NN plane wave contains a deuteron bound-state component. This part, which is absent for charged-pion production, is automatically excluded as soon as the NN interaction is switched on, because the scattering state is orthogonal to the deuteron ground state. The second source is the change in the radial wave function of the final NN partial waves by the interaction. The latter is also responsible for the reduction of the charged-pion channels.

Figure 9 shows a comparison of our results for the total cross-sections for π^- and π^0 photoproduction with experimental data. In view of the fact that data for π^+ production in the Δ region are not available, we concentrate the discussion on π^- and π^0 data. In the case of π^- production we have taken the experimental data from [6, 29,30] while for π^0 production we compare our results with the experimental data from [8]. One readily notes, that in agreement with earlier results the pure IA cannot describe the experimental data, especially in the case of π^0 production. The inclusion of such effects improves the agreement between experimental data and theoretical predictions considerably. Only in the maximum of π^0 production our model overestimates the measured total cross-section by about 6%.

Finally, we compare our results with the theoretical predictions from [10] as shown in fig. 10. Surprisingly, one notes for the impulse approximation a significant difference for charged-pion production which cannot be attributed to the use of different elementary production operators. A possible explanation for this feature will be presented in the next section, where we will discuss the differential cross-sections. On the other hand, inclusion of FSI leads in our case to a reduction, whereas an enhancement was found in [10] for charged-pion production. As a result, one finds quite close agreement for the two calculations, if FSI is included. On the contrary, for neutral pion production we obtain reasonable agreement in the IA with [10], only in the maximum and at higher energies

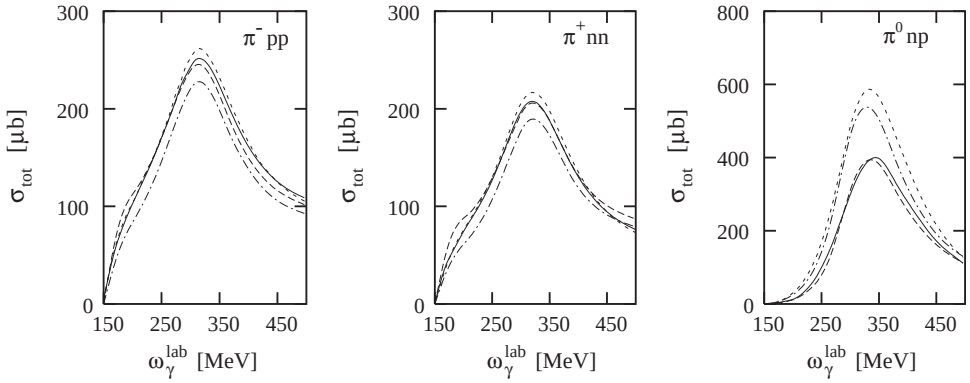

Fig. 10. Total cross-sections for pion photoproduction on the deuteron. Short-dashed curves: IA of present calculation; solid curves: IA plus NN and πN rescattering of present calculation; dash-dotted curves: IA of Levchuk *et al.* [10]; dashed curves: IA plus NN rescattering from [10].

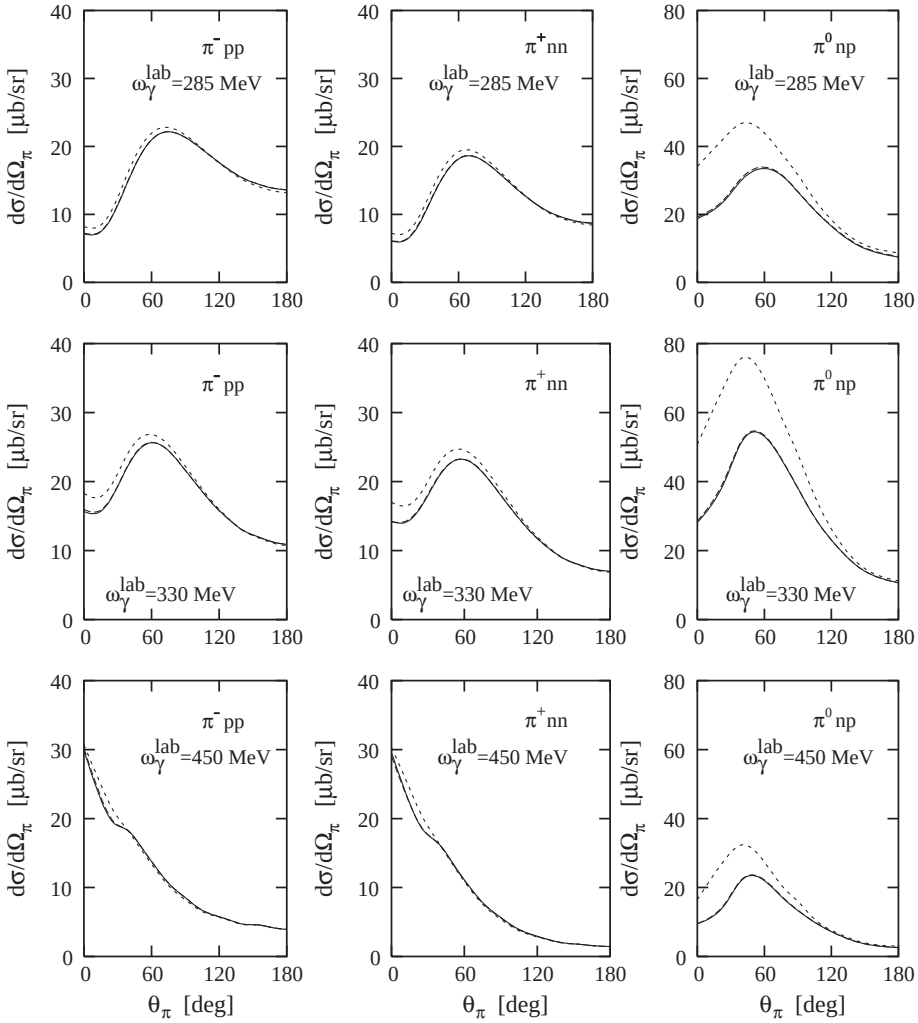

Fig. 11. Differential cross-sections for pion photoproduction on the deuteron for various energies. Short-dashed curves: IA; dashed curves: IA plus NN rescattering; solid curves: IA plus NN and πN rescattering. The left, middle and right panels represent the differential cross-section for $\gamma d \to \pi^- pp$, $\pi^+ nn$ and $\pi^0 np$, respectively.

one notes some differences which very likely come from the neglect of higher resonances in our elementary photoproduction model. Both calculations predict a strong reduction by FSI leading to a satisfactory agreement. The remaining small differences probably stem from different pion photoproduction operators and from different realistic NN potential models, since in [10] the Bonn r-space potential model [11] has been used.

5.2 Differential cross-section

We begin the discussion by presenting the results for the differential cross-sections in the pure IA and with rescattering included in fig. 11. Here one sees that the major contribution from FSI appears at forward pion angles, *i.e.*, at angles less than 90°, predominantly from NN rescattering, whereas rescattering effects become quite small for backward angles. As already noted for the total cross-section, the overall effect is quite small for charged pions, reaching a maximal reduction at $\theta_\pi = 0°$ of about 15% and decreasing rapidly with increasing angle. In the case of the π^0 channel, the results for the total cross-section have already shown that the effect of rescattering is large. Again one notes that the dominant effect appears at forward pion angles resulting in a strong reduction of the order of 40%. At 90° the reduction is still sizeable but decreases to a tiny effect at 180°.

Another interesting feature is that for charged-pion production in contrast to π^0 production the angular distribution of the emitted pion is more and more forward peaked with increasing photon energy. Its origin are the Born terms which are absent for π^0 production. This is demonstrated in fig. 12 where the separate contributions from Born and resonance terms are shown. More than 70% of the differential cross-section at $\theta_\pi = 0$ comes from the Born terms.

A comparison with experimental data from [6] for π^- production and from [8] for π^0 production is shown in figs. 13 and 14. Since in [8] the differential cross-sections for the reaction $d(\gamma,\pi^0)np$ are given in the so-called γN c.m. frame, we have transformed the differential cross-sections from the lab frame to the γN c.m. frame. The pion angle in the γN c.m. frame is denoted by $\theta_\pi^\star$.

For π^- production the small reduction at forward angles leads at 350 MeV to an improved and satisfactory description of the data at forward angles. At the lower energy of 250 MeV FSI effects are small, but one notes in the maximum around 90° an underestimation of the data by about 15%, while at 180° the theory is slightly higher than the data. Also at 420 MeV the theory is at forward angles slightly above the data but below in the backward direction. However, the overall description is quite satisfactory. The comparison between theory and experiment is even better for π^0 production, where the inclusion of FSI yields an almost perfect description.

Now we compare our results for the differential cross-sections with the theoretical predictions of Levchuk *et al.* [10] in fig. 15. For the π^0 channel we find quite a good agreement in the maximum. At forward angles one notes

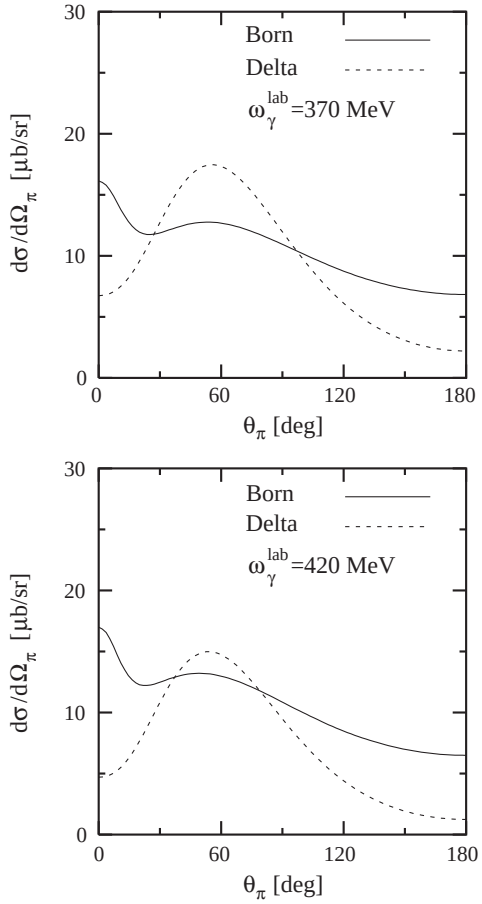

Fig. 12. Differential cross-section for π^- photoproduction on the deuteron in impulse approximation. Solid curves: contribution of Born terms alone; short-dashed curves: contribution of the $\Delta(1232)$-resonance alone.

for the pure IA as well as with inclusion of FSI only at the lowest energy agreement, whereas for the two higher energies larger differences appear. In the backward direction we find for all three energies a significantly larger cross-section already for the IA while FSI effects are tiny (see right panels of fig. 15). Again we suspect differences in the elementary production amplitude to be responsible for this fact. However, for charged-pion production the situation is quite different. Major discrepancies are evident in the forward direction for the IA. While we find an increased forward peaking of the cross-section with increasing energy, the cross-section remains small in [10] at $\theta_\pi = 0$. Analysing in detail the contributions from the $s = 0$ and $s = 1$ parts of the NN final-state plane wave (see left panel of fig. 16), we discovered that we could reproduce the results of [10] if we assume a wrong antisymmetrization for the $s = 0$ channel, *i.e.*, using instead of (11) for $s = 0$

$$|\vec{p}_1\vec{p}_2,00,t-\mu\rangle = \frac{1}{\sqrt{2}}\big(|\vec{p}_1\rangle^{(1)}|\vec{p}_2\rangle^{(2)} + (-)^t|\vec{p}_2\rangle^{(1)}|\vec{p}_1\rangle^{(2)}\big)|00,t-\mu\rangle\,, \quad (35)$$

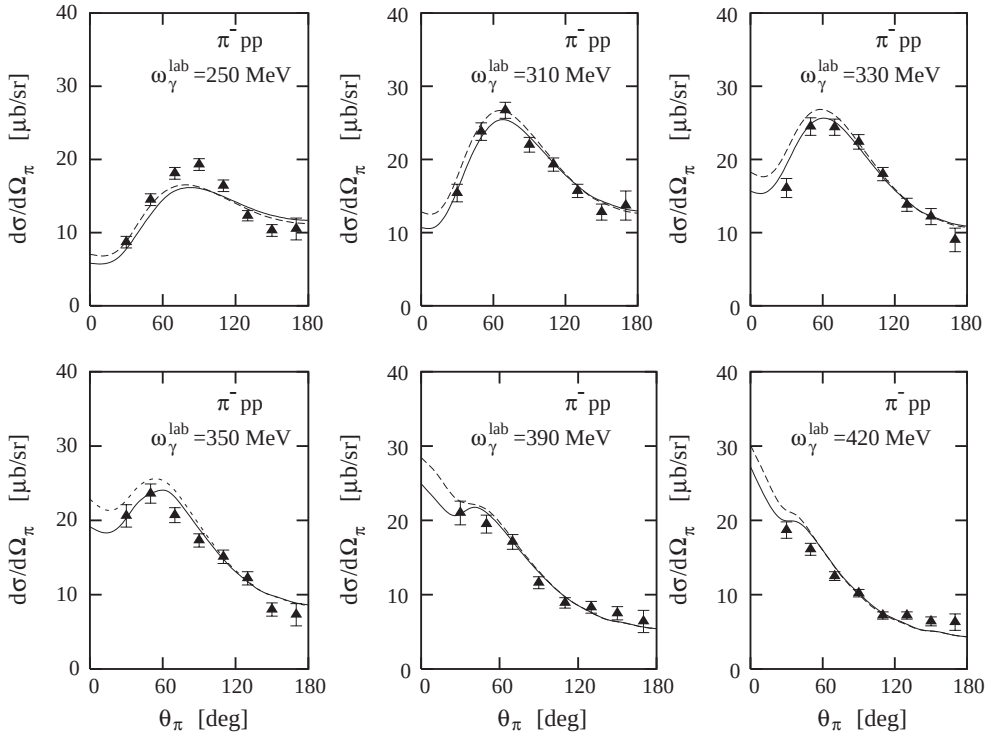

Fig. 13. Differential cross-sections for π^- photoproduction on the deuteron. Solid curves: IA plus NN and πN rescattering; dashed curves: IA. Experimental data: [6].

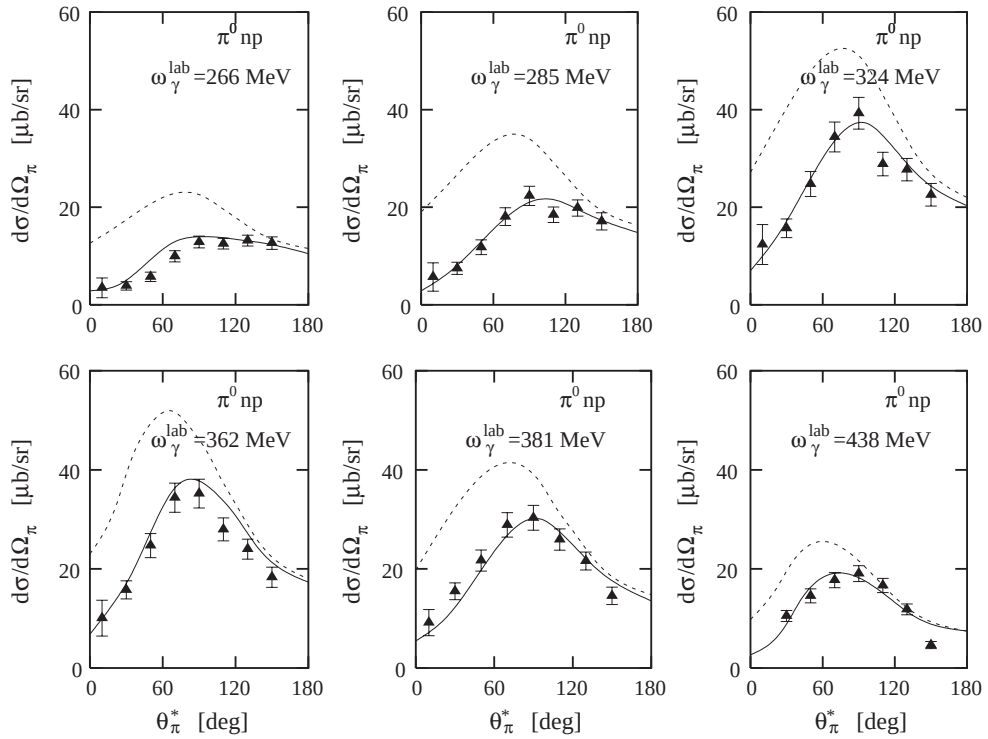

Fig. 14. Differential cross-sections for π^0 photoproduction on the deuteron. Solid curves: IA plus NN and πN rescattering; dashed curves: IA. Experimental data: [8].

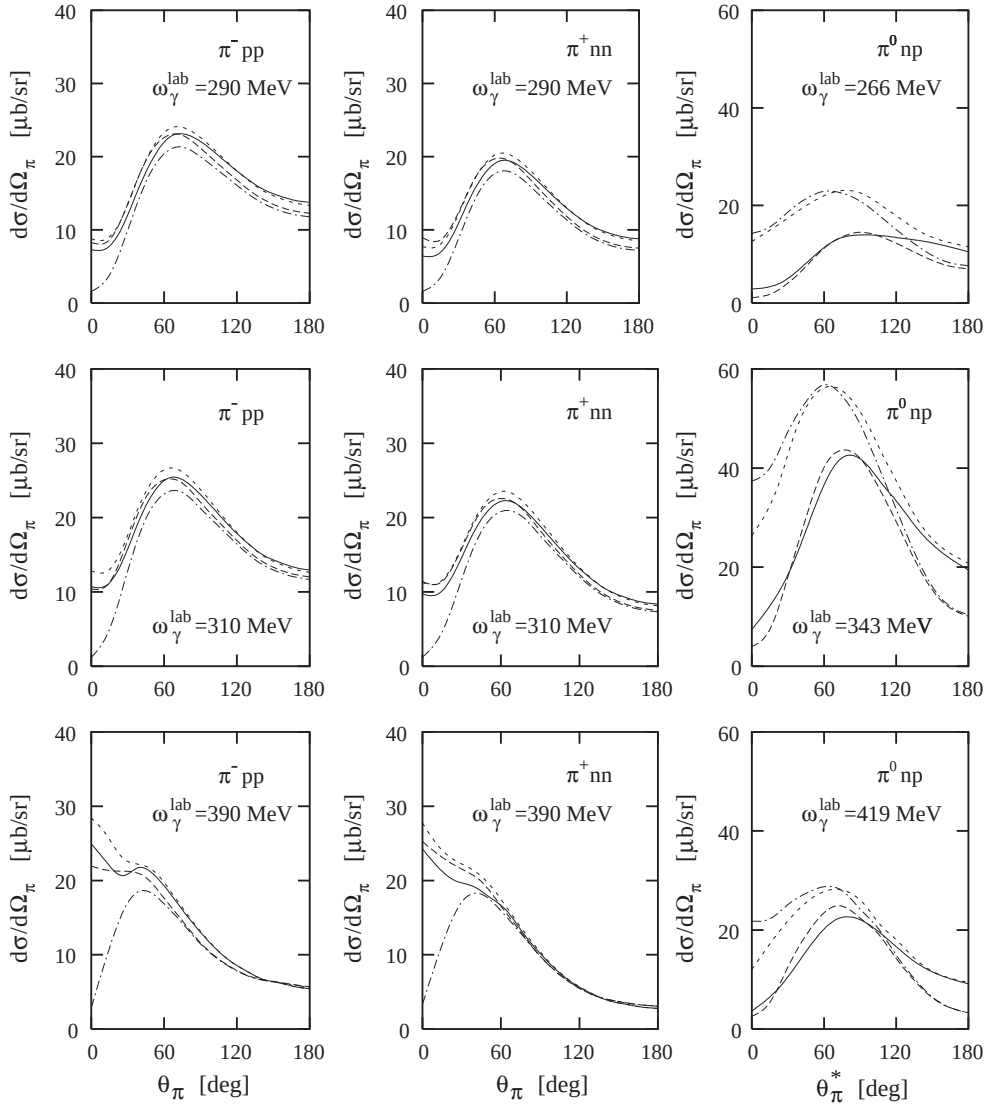

Fig. 15. Differential cross-sections for pion photoproduction on the deuteron in comparison with the results from [10] at different photon energies. Solid curves: our results for IA plus NN and πN rescattering; short-dashed curves: our results in IA; dashed and dash-dotted curves: results from [10] with and without rescattering effects, respectively.

and keeping the form of (11) for the $s = 1$ channel. This is demonstrated in the right panel of fig. 16, where we obtain in this case also a decrease of the cross-section at 0° very similar to [10]. This wrong antisymmetrization for the $s = 0$ channel corresponds in the uncoupled representation, as used in [10], to an interchange of the momenta of the two nucleons alone without interchanging the spin quantum numbers. This we have checked by using also an uncoupled, *i.e.*, helicity basis leading to the same result. However, we can only suspect that the difference to the results of [10] may originate from such an error in the antisymmetrization.

6 Summary and conclusions

In this work we have investigated the influence of final-state interaction effects on incoherent single-pion photoproduction on the deuteron in the $\Delta(1232)$-resonance region. The elementary production operator on the nucleon is taken in an effective Lagarangian model used earlier in a study of the same process in the impulse approximation, where all kind of final-state interactions and other two-body operators were neglected. As presumably dominant final-state interaction effects we have included the complete rescattering contributions in the two-body NN- and πN-subsystems. As models for the interaction of the NN- and πN-subsystems we used separable representations of realistic NN and πN interactions which give a good description of the corresponding phase shifts. For NN rescattering, we have included all partial waves with total angular momentum $J \leq 3$ and for πN rescattering S- through D-waves.

We found that the influence of NN and πN rescattering reduces the total cross-sections in the $\Delta(1232)$-

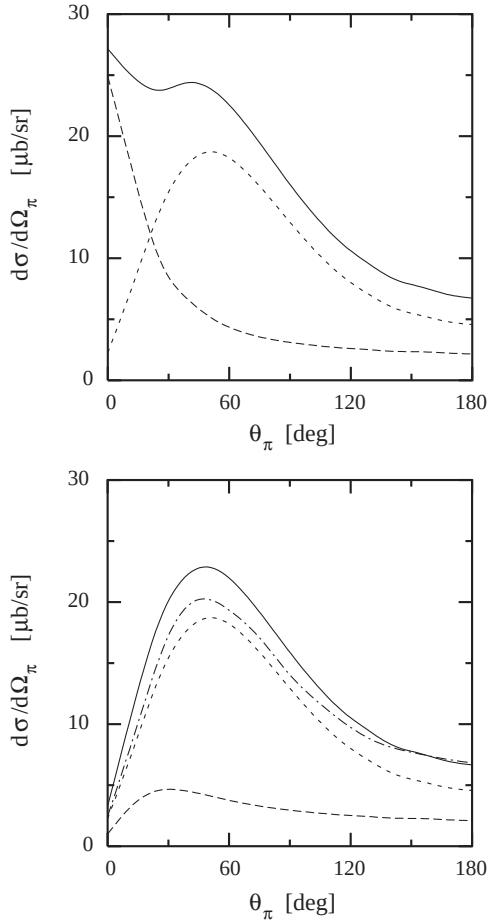

Fig. 16. Differential cross-section for π^- photoproduction on the deuteron in the impulse approximation at a photon energy of 370 MeV. Upper panel: our result with separate $s = 0$ (dashed curve) and $s = 1$ (short-dashed curve) contributions; solid curve: total result; lower panel: our result assuming a wrong NN antisymmetrization for the $s = 0$ channel (see (35)). Notation as in the upper panel. In addition the result of [10] (dash-dotted curve).

resonance region for charged-pion photoproduction by about 5% and for π^0 photoproduction reaction, where rescattering is much more important, by about 35% in the maximum. Furthermore, πN rescattering appears to be much less important compared to NN rescattering. In comparison with experimental data, the inclusion of rescattering effects leads to an improved agreement with experimental data. Only in the maximum of π^0 production our model overestimates slightly the measured total cross-section by a few percent. With respect to the theoretical predictions of [10], we obtained very similar results when FSI is included.

The study of the differential cross-section revealed that the reduction by inclusion of FSI appears predominantly at pion forward angles by about 15% for charged-pion production and for the π^0 channel by about 40%. For pions emitted in the backward direction the influence of rescattering is much less important. As already noted for the total cross-section, πN rescattering has a very small effect on the final results. In comparison with experiment, the inclusion of FSI yields a very satisfactory agreement with data. Small discrepancies remain at backward pion angles. In comparison with the results of [10] in the IA, we found for charged-pion channels at forward angles a large difference between both calculations. A detailed analysis gave as possible explanation a wrong antisymmetrization for the final two-proton or two-neutron state. After inclusion of rescattering effects we obtained a satisfactory agreement with [10].

The present study will serve as a basis for further investigations including a three-body treatment of the final πNN system for the lowest and most important partial waves. This will insure the important unitarity condition and may result in an even better agreement between experimental data and theoretical predictions for π^0 photoproduction. A further interesting topic concerns the study of polarization observables giving more detailed information on the dynamics and thus providing more stringent tests for theoretical models. As future refinements we consider also the use of a more sophisticated elementary production operator, which will allow one to extend the present approach to higher energies, and the role of irreducible two-body contributions to the e.m. pion production operator, *e.g.* interaction of the intermediate particle of the nucleon and Δ pole diagrams with the spectator nucleon. In the long run, one would also need to extend the formalism to the threshold region for which the elementary production operator has to be improved. This process is of great interest since experimental data for the reaction $d(\gamma, \pi^0 n)p$ have been measured recently in Mainz (MAMI/TAPS) and Saskatoon (SAL) [31]. Moreover, the formalism should be extended to investigate coherent and incoherent electroproduction of pions on the deuteron including final-state interaction effects in both the threshold and the $\Delta(1232)$-resonance regions in order to analyze recent results from MAMI [32].

We would like to thank Alexander Fix for useful discussions and a critical reading of the manuscript. E.M. Darwish acknowledges a fellowship from Deutscher Akademischer Austauschdienst (DAAD) and would like to thank the Institut für Kernphysik of the Johannes Gutenberg-Universität, Mainz for the very kind hospitality. This work was supported by the Deutsche Forschungsgemeinschaft (SFB 443).

References

1. G.F. Chew, H.W. Lewis, Phys. Rev. **84**, 779 (1951).
2. M. Lax, H. Feshbach, Phys. Rev. **88**, 509 (1952).
3. I. Blomqvist, J.M. Laget, Nucl. Phys. A **280**, 405 (1977).
4. J.M. Laget, Nucl. Phys. A **296**, 388 (1978).
5. J.M. Laget, Phys. Rep. **69**, 1 (1981).
6. P. Benz *et al.*, Nucl. Phys. B **65**, 158 (1973).
7. M.I. Levchuk, V.A. Petrun'kin, M. Schumacher, Z. Phys. A **355**, 317 (1996).
8. B. Krusche *et al.*, Eur. Phys. J. A **6**, 309 (1999).
9. M.I. Levchuk, M. Schumacher, F. Wissmann, Nucl. Phys. A **675**, 621 (2000).
10. M.I. Levchuk, M. Schumacher, F. Wissmann, nucl-th/0011041.

11. R. Machleidt, K. Holinde, Ch. Elster, Phys. Rep. **149**, 1 (1987); R. Machleidt, Adv. Nucl. Phys. **19**, 189 (1989).
12. R.A. Arndt *et al.*, SAID via telnet VTINTE.PHYS.VT.EDU.
13. D. Drechsel, O. Hanstein, S.S. Kamalov, L. Tiator, MAID: `http://www.kph.uni-mainz.de/de/MAID/maid2000/`.
14. R. Schmidt, H. Arenhövel, P. Wilhelm, Z. Phys. A **355**, 421 (1996).
15. E. Breitmoser, H. Arenhövel, Nucl. Phys. A **612**, 321 (1997).
16. O. Hanstein, D. Drechsel, L. Tiator, Nucl. Phys. A **632**, 561 (1998).
17. R. Beck *et al.*, Phys. Rev. Lett. **78**, 606 (1997); R. Beck *et al.*, Phys. Rev. C **61**, 035204 (2000); H.-P. Krahn, PhD Thesis, Johannes Gutenberg-Universität, Mainz, 1996.
18. R. Leukel, PhD Thesis, Johannes Gutenberg-Universität, Mainz, 2001.
19. I. Preobrajenski, PhD Thesis, Johannes Gutenberg-Universität, Mainz, 2001.
20. T. Fujii *et al.*, Nucl. Phys. B **120**, 395 (1977).
21. A. Bagheri *et al.*, Phys. Rev. C **38**, 875 (1988).
22. F. Härter, PhD Thesis, Institut für Kernphysik, Johannes Gutenberg-Universität, Mainz, 1996.
23. J.D. Bjorken, S.D. Drell, *Relativistic Quantum Mechanics* (McGraw-Hill, New York, 1964).
24. M. Lacombe *et al.*, Phys. Lett. B **101**, 139 (1981).
25. J. Haidenbauer, W. Plessas, Phys. Rev. C **30**, 1822 (1984).
26. J. Haidenbauer, W. Plessas, Phys. Rev. C **32**, 1424 (1985).
27. S. Nozawa, B. Blankleider, T.-S.H. Lee, Nucl. Phys. A **513**, 459 (1990).
28. J.H. Koch, R.M. Woloshyn, Phys. Rev. C **16**, 1968 (1977).
29. G. Chiefari, E. Drago, M. Napolitano, C. Sciacca, Lett. Nuovo Cimento **13**, 129 (1975).
30. M. Asai *et al.*, Phys. Rev. C **42**, 837 (1990).
31. D. Hornidge, Invited talk at the *LOWq Workshop, August 23-25, 2001, Halifax, Nova Scotia, Canada*.
32. H. Merkel, Prog. Part. Nucl. Phys. **44**, 433 (2000).